Advances in Magnetics

Analysis, Design, and Characterization of Ferrite EMI Suppressors

Mirjana Damnjanović[1], Goran Stojanović[1], Vladan Desnica[1], Ljiljana Živanov[1], Ramesh Raghavendra[2], Pat Bellew[2], and Neil Mcloughlin[2]

[1]Department of Electronics, Faculty of Technical Sciences, University of Novi Sad, 21000 Novi Sad, Serbia and Montenegro
[2]Littelfuse Ireland Limited, Dundalk, Co. Louth, Ireland

In this paper design, modeling and characterization of single and double coils, which consist of conductive layer embedded in the soft ferrite material, are described. These surface-mount components, comprising of a cofired multilayered ferrite and coil, have been developed in the ceramic coprocessing technology. A simple analytical model of proposed structures is presented. This model is very suitable for circuit simulations and for prediction of frequency characteristics of considered inductors. The inductance and impedance of coils embedded in low permeability or high permeability ferrite material are calculated and compared. Also, these suppressors were experimentally tested in the frequency range 1 MHz–3 GHz using an Agilent 4287 A RF LCR meter. The calculated results were in good agreement with the measured ones.

***Index Terms*—EMI suppressor, high-frequency characteristics, impedance and inductance calculation, single and double coils.**

I. Introduction

IN THE FIELD of electromagnetic compatibility (EMC), several trends, directed to functional upgrading or reducing cost of electronic equipment, inevitably also contribute to an increasing level of electromagnetic interference (EMI) emissions. At RF frequencies a miniature coil embedded in ferrite shows high impedance, which suppresses unwanted interference. Miniature inductor (or choke) consists of highly conductive layer embedded in a ferrite monolithic structure, which provides a good magnetic shielding and makes inductor very suitable for high density mounting, usually as surface-mount device (SMD). The size, performance and reliability make SMD chip inductors very attractive for a wide range of applications, such as EMI suppression in universal series bus (USB), low-voltage differential signaling and in other high-speed digital interfaces incorporated in notebooks and personal computers, digital cameras and scanners. In addition, ferrite suppressors have been successfully employed for attenuating EMI in switching power supplies or electronic ignition systems. Ferrite components are efficient and cost effective for the prevention of—and protection against—spurious signals transmitted by conduction and radiation. Suppression components are offered in a number of ferrite materials, optimizing impedance over a wide range of frequencies.

In recent years, many literatures [1]–[7] studied high frequency characteristics of ferrite core and/or magnetic components such as ferrite inductors, based on finite element method or physical analysis. Parasitic effects such as stray capacitance [8], self-resonance and magnetic losses of ferrite [9], etc., play an important role in design of such inductors. An understanding of the high-frequency parasitic and packaging effects can be gained from equivalent circuit description of the inductor [4], [10].

The purpose of this paper is to explore design, modeling and characterization of coils embedded in the soft ferrites. The components have been fabricated using the ceramic coprocessing technology. We have already discussed the characterization and modeling of integrated passive devices in thick film [11] and ceramic coprocessing technology [12], [13]. In this paper results obtained using compact computer program SPIS (Simulator for Planar Inductive Structures) developed as CAD tool for calculation of electrical properties of a single and double coil, are presented. The SPIS simulates effects of ferrite materials and geometrical parameters of planar inductive structures, such as single or double coils. With proposed software tool, designers can predict performance parameters quickly and easily before costly prototypes are built. SPIS software offers substantially reduced time to market, and increases device performance.

In Section II, an analytical model of novel single and double coil structures is presented, along with expressions for the elements used. A simple and efficient CAD tool for calculating electrical properties of coils embedded in the soft ferrite material is proposed. Section III presents design of ferrite EMI suppressors. Results and discussions are given in Section IV, while Section V is the summary.

II. Description of Structures and Their Model

Miniature inductors can be installed as SMD [7]. They are made in EIA standard sizes: 0402, 0603, 0805, 1206, 1210, and 1812, and they have impedance between 6 Ω and 2000 Ω

Digital Object Identifier 10.1109/TMAG.2005.860485

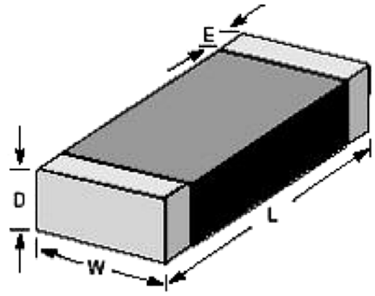

Fig. 1. Typical SMD construction for 1210 chip size.

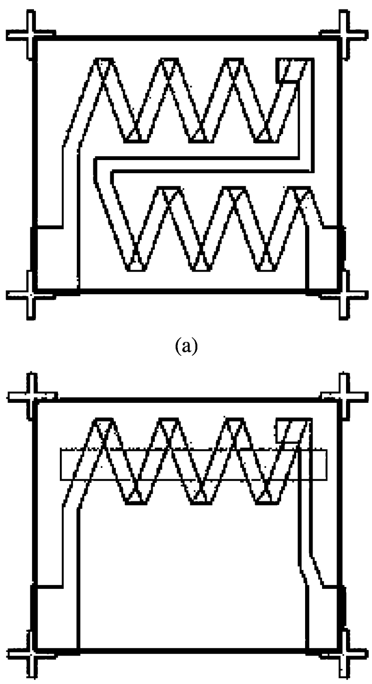

(a)

(b)

Fig. 2. Layout of (a) double coil without core and (b) single coil with core.

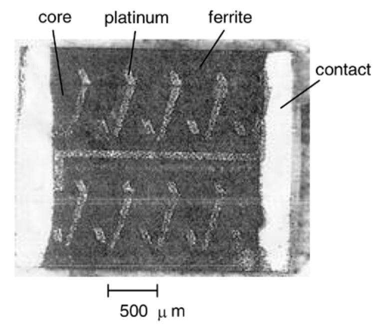

Fig. 3. Cross section of fabricated double coil with core and embedded in ferrite material.

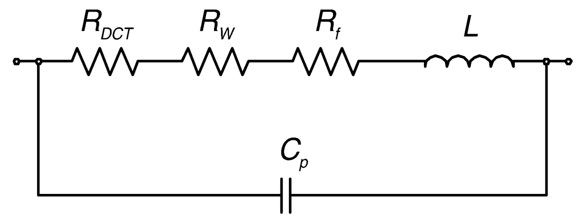

Fig. 4. The lumped parameter equivalent circuit of an inductor embedded in ferrite.

at 100 MHz. The proposed single and double coils structures are realized as surface-mount devices for typical 1210 chip size (Fig. 1). Dimensions referring to the Fig. 1 are as follows: $\mathrm{Dmax} = 2.87$ mm, $\mathrm{E} = 0.50 \pm 0.025$ mm, $\mathrm{L} = 3.20 \pm 0.30$ mm, $\mathrm{W} = 2.54 \pm 0.30$ mm. Layouts of double and single coils are depicted in Fig. 2(a) and (b), respectively. For simplicity, the double coil is depicted without core. Due to low electrical resistivity, platinum Pt ($\rho = 10.6 \cdot 10^{-8}\ \Omega{\cdot}\mathrm{m}$) was chosen as the conductive paste to form the single and double coils. The thickness of platinum layer is 10 μm. The coils are embedded in the middle of a ferrite layer (2.87 mm thick) and the core (if it is embedded) is made from a ferrite layer 6 μm thick. We have fabricated single coil with and without core in low permeability and high permeability ferrite material and all the same for double coil. Fig. 3 shows the cross section of fabricated double coil with the core and embedded in the soft ferrite material. In this figure, the upper ferrite is removed in order to enable visibility of inner configuration of platinum layer. The length of one conductive segment is approximately 950 μm, the width is 170 μm, and the angle between adjacent segments is around 40°.

The soft ferrite materials are used in an extensive range of products and applications. Ferrite components have been used for reducing or eliminating conducted EMI or for attaining an electromagnetic compatibility (EMC). The ferrite material or ferrite core introduces into circuit frequency dependent impedance and inductance. The permeability of the ferrite material is a complex parameter consisting of a real $\mu_r^{'}$ and imaginary part $\mu_r^{''}$,

$$\mu_r(f) = \mu_r^{'}(f) - j \cdot \mu_r^{''}(f). \tag{1}$$

The real component represents the reactive portion and the imaginary component represents the losses. Both parts of the permeability are frequency dependent, as it can be seen in MMG Neosid Ltd. Web Site [14]. The analytical expressions for real $\mu_r^{'}(f)$ and imaginary part $\mu_r^{''}(f)$ are obtained using fitting techniques according to measurement (because of data, which is derived from measurements on toroidal cores and the values obtained [14] cannot be directly transferred to products of another shape and size).

In order to analyze single and double coil with or without ferrite core and embedded in the soft ferrite material, the equivalent circuit describing electrical properties of the presented structure is determined.

Fig. 4 shows the lumped parameter equivalent circuit of an inductor embedded in ferrite material. Resistances R_W and R_f are the winding and ferrite resistances, respectively.

The element R_{DCT} presents the total dc resistance. Inductance L is frequency dependent inductance of inductor (coil) and C_P is the overall parasitic capacitance including the distributed turn-to-turn and turn-to-ferrite stray capacitance.

TABLE I
EQUATIONS OF THE PROPOSED EQUIVALENT MODEL

	Equation
Inductance	
$$L=\sum L_S-\sum\left\|M^-\right\|+\sum M^+$$	(2)
$$L_S(f)=\left(\frac{\mu_0\cdot l}{2\cdot\pi}\right)\left(\mu_r^{'}(f)\cdot\left(\ln\left(\frac{2\cdot l}{w+t}\right)+0.25049+\frac{(w+t)}{3\cdot l}\right)+\frac{T(f)}{4}\right)$$	(3)
$$M=\frac{\mu_o\cdot\mu_r^{'}(f)\cdot l}{2\cdot\pi}\cdot\left(\ln\left(\frac{l}{d}+\sqrt{1+\left(\frac{l}{d}\right)^2}\right)-\sqrt{1+\left(\frac{d}{l}\right)^2}+\frac{d}{l}\right)$$	(4)
$$2M=(M_{l+m\pm\delta}+M_{\delta})-(M_{l\pm\delta}+M_{m\pm\delta})$$	(5)
$$2M=(M_{m+p}+M_{m+q})-(M_p+M_q)$$	(6)
$$M=\frac{\mu_o\cdot\mu_r^{'}(f)}{4\cdot\pi}\cdot cos\varepsilon\cdot\left(2\left[(\mu+l)\cdot arth\frac{m}{R_1+R_2}+(v+m)\cdot arth\frac{l}{R_1+R_4}-\mu\cdot arth\frac{m}{R_3+R_4}-v\cdot arth\frac{l}{R_2+R_3}\right]-\frac{\Omega\cdot d}{sin\varepsilon}\right)$$	(7)
$$\Omega=arctg\left\{\frac{d^2\cdot cos\varepsilon+(\mu+l)\cdot(v+m)\cdot sin^2\varepsilon}{d\cdot R_1\cdot sin\varepsilon}\right\}-arctg\left\{\frac{d^2\cdot cos\varepsilon+(\mu+l)\cdot v\cdot sin^2\varepsilon}{d\cdot R_2\cdot sin\varepsilon}\right\}+$$ $$+arctg\left\{\frac{d^2\cdot cos\varepsilon+\mu\cdot v\cdot sin^2\varepsilon}{d\cdot R_3\cdot sin\varepsilon}\right\}-arctg\left\{\frac{d^2\cdot cos\varepsilon+\mu\cdot(v+m)\cdot sin^2\varepsilon}{d\cdot R_4\cdot sin\varepsilon}\right\}$$	(8)
$$R_1=R(m,l,\mu,v),\ R_2=R(0,l,\mu,v),\ R_3=R(0,0,\mu,v),\ R_4=R(m,0,\mu,v)$$	(9)
$$R(x,y,\mu,v)=\sqrt{d^2+(\mu+y)^2+(v+x)^2-2\cdot(\mu+y)\cdot(v+x)\cdot cos\varepsilon}$$	(10)
Resistance	
$$R=R_{DCT}+R_w+R_f$$	(11)
$$R_{DC}=\rho\frac{l}{w\cdot t}$$	(12)
$$R_w=R_{DC}\cdot A\cdot\left[\frac{e^{2A}-e^{-2A}+2sin(2A)}{e^{2A}+e^{-2A}-2cos(2A)}+2\cdot\frac{N_i^2-1}{3}\cdot\frac{e^{A}-e^{-A}-2sin(A)}{e^{A}+e^{-A}+2cos(A)}\right]$$	(13)
$$R_f=2\cdot\pi\cdot f\cdot L_0\cdot\mu_r^{''}(f)$$	(14)
Capacitance	
$$C_p=l_{tot}\cdot\left[\varepsilon_o\cdot\varepsilon_r\cdot\frac{2\cdot\pi}{ln\left(1+\frac{2\cdot h}{t}+\sqrt{\frac{2\cdot h}{t}\cdot\left(\frac{2\cdot h}{t}+2\right)}\right)}+\varepsilon_o\cdot\varepsilon_r\cdot\frac{w-t/2}{h}\right]$$	(15)

A. Calculation of Self- and Mutual Inductance

In this subsection, the concept of inductance calculation of a single or double inductor is described. The calculation of electrical parameters (inductance, resistance, impedance and Q-factor) of single or double coil is very complex. Therefore, the inductor is divided into segments having small, rectangular cross sections. To obtained the correct total inductance L, the mutual inductance between all segments of inductor has to be calculated and added to the sum of all segments self-inductance L_S [15], [16]. The total inductance L is calculated by (2), as it can be seen in Table I. For straight conductor of rectangular cross section self-inductance is given by the formula (3), where w is conductor width, t is conductor thickness, l is conductor length, and $T(f)$ is frequency dependent factor. In the expression (3) for self-inductance, the constant 0.25049

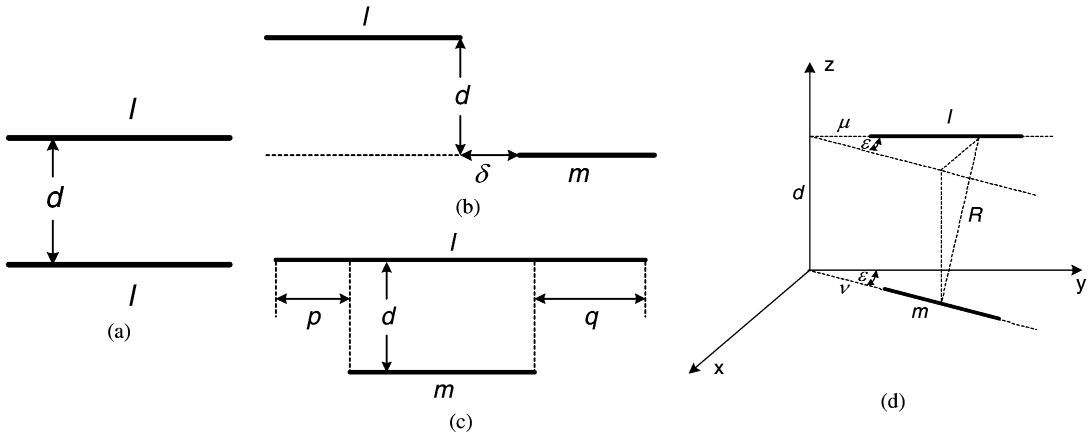

Fig. 5. The possible mutual position of segments of single or double coil.

is a result of using the concept of geometric mean distance (GMD) and arithmetic mean distance (AMD) for conductor with rectangular cross section [15], [17].

This computational concept, of mutual inductance, considers segments as simple filaments. Depending on the current vectors in filaments, the mutual inductance is positive (M^{+}), if the current vectors are oriented in the same direction, or negative (M^{-}) if the current vectors are in opposite directions. The possible configurations in space are illustrated in Fig. 5. The exact formula for calculation of mutual inductance for parallel filaments of equal length shown in Fig. 5(a) is given by (4), where l is the length of each filaments and d is the vertical distance between the filaments in the plane.

Other configurations of parallel segments are based on this equation. When the segments are parallel, several distinct cases may appear. The first is shown in Fig. 5(b) and the mutual inductance is calculated by (5), where δ is positive for nonoverlapping segments and negative for overlapping ones. In the second case, as shown in Fig. 5(c), the mutual inductance between the two conductors with lengths l and m is calculated by (6). Mutual inductance M of two straight segments placed in any desired position [Fig. 5(d)] is calculated by means of formulas as in [17, p. 56] as in (7). In (7), the parameter Ω is given by (8)–(10).

B. Calculation of Resistance

The total resistance R is sum of total dc resistance $R_{\rm DCT}$, winding resistance R_w and ferrite resistance R_f (all elements are shown in Fig. 4). Therefore, resistance R can be expressed as in the formula (11). The total dc resistance is calculated by (12), where ρ is the resistivity of the conductor, t is its thickness, w is its width, and l is its length. Experimental results show that $R_{\rm DCT}$ is several times larger (due to the resistance of the contacts) than the resistance calculated by (12). The contact resistance slightly increases the total dc resistance and its influence is significant only at low frequencies. Therefore, it is modeled as a part of $R_{\rm DCT}$. In our case, for single coil structure, the contact resistance is 7.43 Ω and for double coil is 10.63 Ω. For proposed model shown in Fig. 4, these values are approximately ten times greater than $R_{\rm DC}$ given by (12).

As frequency rise, the resistance of an inductor increases due to the presence of time-varying electromagnetic field, which results in skin and proximity effect. The final result of these two combined effects is reduction in the effective cross-sectional area of the conductive layer available for the current flow. Therefore, ac resistance (or winding resistance) at high frequencies becomes greater than dc resistance, and it can be calculated by (13), where A is factor which depends on winding geometry. The first and second term represent skin effect and proximity effect in the winding, respectively. For a strip wire, with dimensions w and t, A becomes $A = (w/\delta)\sqrt{(t/p)}$, where p is the distance between the centers of two adjacent conductors ($p \approx t$ for right conductive segment). Skin depth δ of wire is expressed as $\delta = \sqrt{(\rho/\pi \cdot \mu_o \cdot f)}$. The lumped parameter R_f from Fig. 4 is given by (14), where f is the operating frequency; L_0 is the inductance of inductor in vacuum and $\mu_r''(f)$ is the imaginary part of complex permeability.

C. Calculation of Capacitance

The expression for parasitic capacitance C_P (element of inductor's model shown in Fig. 4) is given by closed form expression (15), similarly as in [18], where are $l_{\rm tot}$—the total length of segments of conductor, t—the thickness of conductor, w—the width of conductor, and $h = 0.5\cdot$ (the width of ferrite layer). All above mentioned parameters are given in centimeters. Thus, in accordance with (15), the capacitance is obtained in fF.

D. Calculation of Impedance

The impedance of the inductor depends of the geometry of the conductive material and ferrite core, and of the permeability of the ferrite material μ. At low frequencies losses in inductor are low. Losses start to increase as frequency increases; at ferrimagnetic resonant frequency the inductor behaves as a frequency-dependent resistor and no longer as a true inductance. This is very important in elimination of conducted EMI [19]. Due to the presence of ferrite material, total impedance has reactive and resistive part. The real part corresponds to the reactance, positive for an inductance, negative for a capacitance, and the imaginary part to the losses. The formula for impedance is given as

$$|Z| = \sqrt{R^2 + (2 \cdot \pi \cdot f \cdot \mu_r'(f) \cdot L_0)^2}. \qquad (16)$$

E. Calculation of Quality Factor

For equivalent circuit of inductor as in Fig. 4, the quality factor is

$$Q = \frac{\mathrm{Im}(Z)}{\mathrm{Re}(Z)} = \frac{\omega \cdot L}{R} \cdot (1 - \omega^2 \cdot L \cdot C_P) - \omega \cdot R \cdot C_P. \quad (17)$$

III. Design of Ferrite EMI Suppressors

The proposed software tool is developed for simulation of characteristics of single or double coils, which consist of conductive layer embedded in soft ferrite material. The first step in designing the ferrite EMI suppressor is to select one of the standard sizes of SMD chip inductors. After that, the ferrite material, which can provide the best performance of suppressor, has to be chosen.

A. Selection of SMD Ship Size

In our software tool, user can select one of the standard sizes for SMD inductor:

- 1210, shown in Fig. 1;
- 1206; or
- 0805.

B. Selection of Soft Ferrite Material

If the selection of ferrite material has to be taken, it is necessary to take care of the range of unwanted frequencies that can occur. We have tested two soft ferrite materials, which have remarks **LP** (***low permeability*** *ferrite material*) and **HP** (***high permeability*** *ferrite material*). These materials are available commercially by Neosid [14]. The LP nickel-zinc ferrite has low loss factors at medium frequencies and high suppression impedance at high frequencies (over 100 MHz). The HP ferrite material is nickel–zinc ferrite, with initial permeability 1000 (while, LP has initial permeability 220). Typical applications for these ferrite materials are in EMI suppressors.

C. Selection of Conductive Material

Outside the range of frequencies where conducted EMI has to be eliminated, the inductor must have low losses. To obtain that goal, for conductive layer has to be chosen material with high conductivity. In SPIS parameters for platinum (Pt) and silver-palladium (PdAg) are included (Du Pont) [20]. In addition, the user can set desired values for conductivity (or resistivity) value of conductive paste directly in the field for input data.

D. Selection of a Structure of Inductor

Besides the characteristics of materials, as mentioned before, the geometry of conductive layer determines the total inductance or impedance, also. Because of that, it is very important to choose appropriate geometrical structure of inductor. The analyzed structures of inductors are shown in Fig. 2. The conductive layer has a single coil or double coil type structure. In addition, the user can set desired values for simple straight conductive line (length l, width w, thickness t) and, also, the angle between adjacent segments of conductor.

On the basis of the all initial values for input data, the program will determine the maximal number of turns $N_{\max}$ on available chip size. The parameter $N_{\max}$ gives information how much (maximum) conductive segments with corresponding angle between them may be set on available chip area, which is defined by the standard SMD chip size. The user can choose number of turns N not greater than $N_{\max}$.

The simulation tool SPIS offers many possibilities to design the EMI suppressor with best performance.

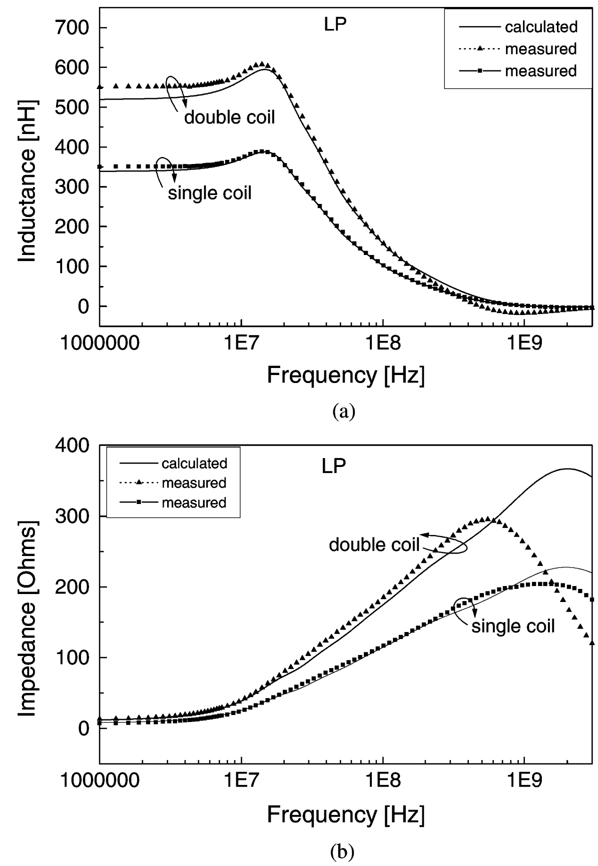

Fig. 6. Frequency dependence of (a) the inductance and (b) the impedance for single and double coil in LP ferrite.

IV. Results and Discussion

To obtain the optimal design of inductor, it is much more convenient to use some simulation tool, than make a specific test component. Because of that, the simulation tool SPIS for calculation of inductance and impedance of ferrite EMI suppressor is developed.

As a result of the conducted simulations, calculated values can be presented:

- total inductance L versus frequency f;
- total impedance Z versus frequency f.

The measurement and characterization of the components was performed with an Agilent 4287 A RF LCR meter for frequencies up to 3 GHz.

The inductance and impedance versus frequency are plotted in Fig. 6(a) and (b) (without ferrite core), and in Fig. 7(a) and (b) (with ferrite core), respectively, for LP soft ferrite material.

The measured and calculated inductance and impedance versus frequency are illustrated in Fig. 8(a), and (b),

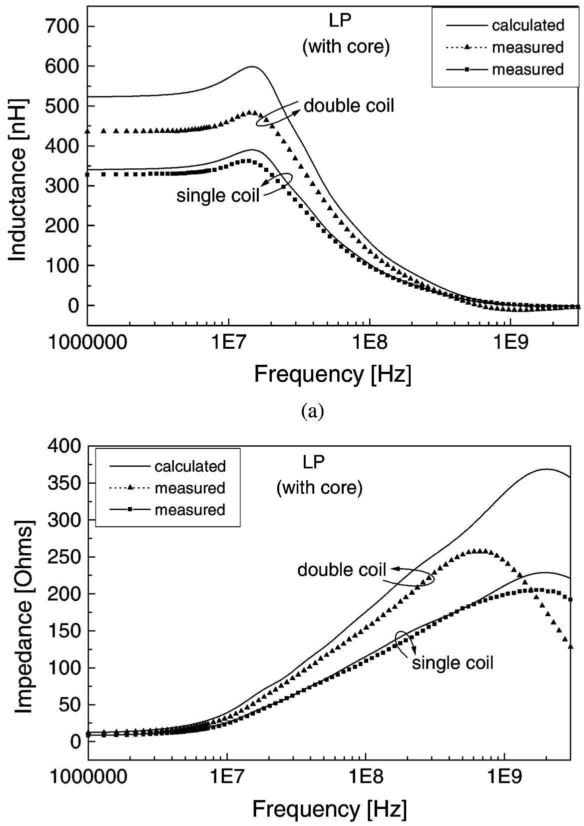

Fig. 7. Frequency dependence of (a) the inductance and (b) the impedance for single and double coil in LP ferrite with core.

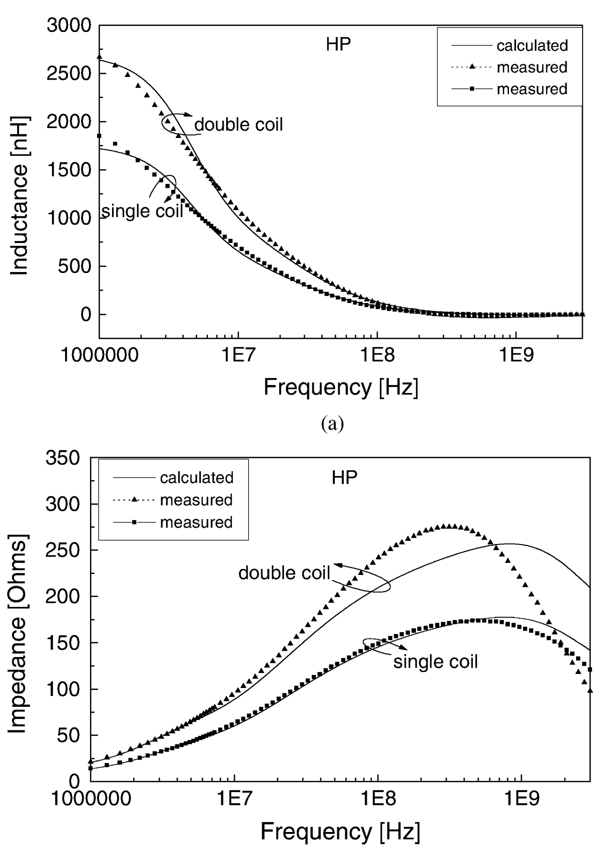

Fig. 8. Single and double coil in HP ferrite measured and calculated (a) inductance and (b) impedance.

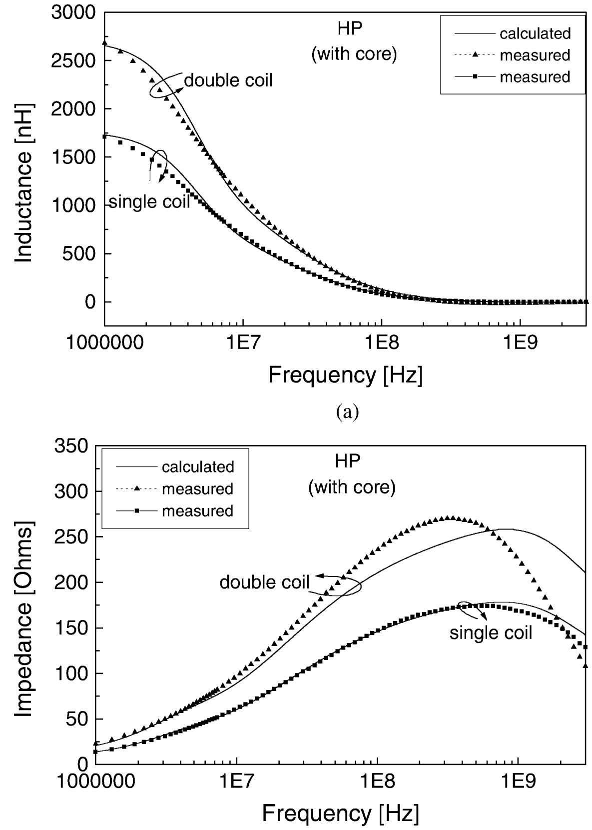

Fig. 9. Single and double coil (with core) in HP ferrite measured and calculated (a) inductance and (b) impedance.

(without ferrite core), and in Fig. 9(a) and (b) (with ferrite core), respectively, for HP soft ferrite material.

The single and double coils employed in this paper generate well-localized magnetic fields existing only in the vicinity of the coil plane. Therefore, the electromagnetic field is confined in sandwich structure, hence resulting in virtually no electromagnetic interference to other low-energy level components in the electronic systems.

As can be seen from previous figures, structures in HP ferrite material have wider frequency range with high impedance. That means, LP ferrite material is more frequency selective for application in EMI suppressors and it has the greater maximal value of impedance. As we expected, double coil has the greater values of inductance and impedance than single coil in both ferrite material. If thin ferrite core is added between conductive segments, the values of impedance are slightly increased. This effect is more significant for structures in HP ferrite material. HP ferrite material has greater value of initial permeability than LP material, and hence, coils with this ferrite have greater inductance values, especially at low frequencies. Cofiring of ceramics is not easy and is fraught with difficulty. Material diffusion or contamination is also a key concern when dealing with electrical properties. The diffusion of Pt into the ferrite material can result in deterioration of both the ferrite material characteristics and the conductor material characteristics. This phenomenon is not possible to be included into the model successfully. Thus, deviation of the impedance measurement results compared to the cal-

TABLE II
NUMERICAL INPUT DATA AND CALCULATED VALUES OF THE MODEL PARAMETERS AND ELECTRICAL PARAMETERS FOR SINGLE COIL WITHOUT CORE, AT 1 GHz

Input parameters	
The length of one Pt segment	950 μm
The angle between adjacent segments	40°
The number of segments	7
The width of conductor	170 μm
The thickness of conductor	10 μm
The width of ferrite layer	2540 μm
The thickness of ferrite layer	2870 μm
Model parameters	
R_{DCT}	7.43 Ω
R_w	20.51 Ω
R_f	181.96 Ω
R	209.87 Ω
L	1.51 nH
C_p	19.81 fF
Electrical parameters	
Z	210.13 Ω
Q	1.92

culated ones in the range around 1 GHz is a consequence above reasons, and this deviation is greater in the case of a double coil. The double coil, naturally, has greater the total length of conductor (Pt) than single coil, as it can be seen from their layouts in Fig. 2. Because of that, the double coil has larger area in which the diffusion of Pt into the ferrite material is significant and consequently this effect is harder to estimate in the case of double coil. We can see that the impedance has peak at the resonant frequency and the ferrite is effective in a wide frequency band around it. The ferrite material choice depends on critical interference frequencies. Ideally they should coincide with the ferrimagnetic resonance frequency, where impedance curve has maximum. The higher the interference frequency, the lower the ferrite material permeability should be. The whole RF spectrum can be covered with a few ferrites if the right permeability steps are chosen.

The proposed model allows that all the parameters affecting the single or double coil structure to be accurately predicted and controlled during design process. For illustration, some of input data and calculated values of the model parameters, for single coil embedded in the LP ferrite material (without core), at operating frequency 1 GHz, are summarized in Table II.

Characterization of inductor using simulation is much more flexible, avoiding the need for a specific test component. Because simulation adds predictive nature to the design process, changes can be made more easily to optimize and fine-tune the layout of the inductor or to improve the choice of the appropriate ferrite material.

When we compare proposed single and double coil embedded in ferrite material with commercial surface mount components for the same application (in 1210 chip size), we may bring the following conclusion. The proposed surface mount components have greater impedance value, for example, at frequency 100 MHz, impedance range is from 95 to 240 Ω, while commercial surface mount chip an EMI suppressor MB1210 [21] have impedance range from 31 to 60 Ω at frequency 100 MHz. This reason thus recommends that our structures can be used as EMI suppressors, very successfully.

V. CONCLUSION

Miniature inductors consisting of coils embedded in the soft ferrite material, find useful application in the suppression of EMI at RF frequencies. In this paper, the design, modeling, and characterization of single and double coils embedded in the LP and HP nickel–zinc ferrite materials have been discussed. As can be seen, presented results enable the application of the proposed components in EMI/EMC suppression of induced and conductive EM noise in secondary step of EMI suppression. An accurate description of the frequency response of single and double coils is achieved by means of simple equivalent circuit model. The model allows that all the parameters affecting the inductor electrical properties to be accurately predicted and controlled during the inductor design. First step in designing the inductor with best performances is to make the proper selection of ferrite material, in order to eliminate conducted EMI. It would be ideal to choose ferrite material, which has the ferrite resonant frequency in the range of unwanted frequencies. Besides ferrite material, the geometry of the inductor also determines the total inductance or impedance. Once the structure and dimensions of inductor are chosen (standard sizes for SMD inductor 1210, 1206, or 0805), it is necessary to set the conductor's length l, width w, thickness t, and angle between adjacent conductor segments. The simulation results will be very useful for construction of the ferrite EMI suppressors. Calculated and measured results show very good agreement over the frequency range from 1 MHz to 1 GHz.

ACKNOWLEDGMENT

This work was supported by Littelfuse Ireland Limited, Dundalk, Ireland. The authors would like to acknowledge Littelfuse Ireland Limited for continuous support and understanding during the project.

REFERENCES

[1] K. Naishadham, "A rigorous experimental characterization of ferrite inductors for RF noise suppression," in *IEEE Radio and Wireless Conf.*, Aug. 1–4, 1999, pp. 271–274.

[2] J. Y. Hsu, H. Ch. Lin, H. D. Shen, and Ch. J. Chen, "High frequency multilayer chip inductors," *IEEE Trans. Magn.*, vol. 33, no. 5, pp. 3325–3327, Sep. 1997.

[3] M. K. Kazimierczuk, G. Sancineto, G. Grandi, U. Reggiani, and A. Massarini, "High-frequency small-signal model of ferrite core inductors," *IEEE Trans. Magn.*, vol. 35, no. 5, pp. 4185–4191, Sep. 1999.

[4] M. Bartoli, A. Reatti, and M. K. Kazimierczuk, “Modeling iron-powder inductors at high frequencies,” in *IEEE Industry Applications Soc. Annu. Meeting*, Oct. 1994, pp. 1225–1232.
[5] U. Reggiani, G. Grandi, G. Sancineto, M. K. Kazimierczuk, and A. Massarini, “High-frequency behavior of laminated iron-core inductors for filtering applications,” in *Applied Power Electronics Conf. Expo.*, Feb. 2000, pp. 654–660.
[6] A. Reatti and M. K. Kazimierczuk, “Comparison of various methods for calculating the AC resistance of inductors,” *IEEE Trans. Magn.*, vol. 38, no. 3, pp. 1512–1518, May 2002.
[7] K. Naishadham, “Experimental equivalent-circuits modeling of SMD inductors for printed circuit applications,” *IEEE Trans. Electromagn. Compat.*, vol. 43, no. 4, pp. 557–565, Nov. 2001.
[8] A. Massarini and M. K. Kazimierczuk, “Self-capacitance of inductors,” *IEEE Trans. Power Electron.*, vol. 12, no. 4, pp. 671–676, Jul. 1997.
[9] K. Liu, T. W. Law, P. L. Cheng, I. T. Chong, and D. C. C. Lam, “Low temperature processing and electrical properties of embedded ferrite-cored inductor,” in *Electronic Components and Technology Conf.*, 2002, pp. 490–494.
[10] Q. Yu, T. W. Holmes, and K. Naishadham, “RF equivalent circuit modeling of ferrite-core inductors and characterization of core materials,” *IEEE Trans. Electromagn. Compat.*, vol. 44, no. 1, pp. 258–262, Feb. 2002.
[11] V. Desnica, Lj. Živanov, O. Aleksić, M. Luković, and M. Nimrihter, “A comparative characteristics of thick film integrated LC filters,” *IEEE Trans. Instrum. Meas.*, vol. 51, no. 4, pp. 570–576, Aug. 2002.
[12] R. Raghavendra, P. Bellew, and N. Mcloughlin, “Coprocessing of electroceramics technology: A simple IPD for combined transient & EMI suppression applications,” *Passive Comp. Ind.*, pp. 13–17, Jan./Feb. 2002.
[13] R. Raghavendra, P. Bellew, N. Mcloughlin, G. Stojanović, M. Damnjanović, V. Desnica, and Lj. Živanov, “Characterization of novel varistor + inductor integrated passive devices,” *IEEE Electron Device Lett.*, vol. 25, no. 12, pp. 778–780, Dec. 2004.
[14] MMG Neosid [Online]. Available: http://www.mmggb.com/pdfs/mmg-Materials.pdf
[15] H. M. Greenhouse, “Design of planar rectangular microelectronic inductors,” *IEEE Trans. Parts, Hybrids, Packag.*, vol. PHP-10, no. 2, pp. 101–109, Jun. 1974.
[16] S. Stalf, “Printed inductors in RF consumer applications,” *IEEE Trans. Consum. Electron.*, vol. 47, no. 3, pp. 426–435, Aug. 2001.
[17] F. W. Grover, *Inductance Calculations, Working Formulas and Tables*. Princeton, NJ: D. van Nostrand, 1946. Reprinted by Dover Publications, New York, 1954.
[18] C. P. Yuan and T. N. Trick, “A simple formula for the estimation of two-dimensional interconnects in VLSI circuits,” *IEEE Electron Device Lett.*, vol. EDL-3, no. 12, pp. 391–393, Dec. 1982.
[19] M. Mardiguian, *EMI Troubleshooting Techniques*. New York: McGraw-Hill, 2000.
[20] DuPont Technical Information [Online]. Available: http://www.dupont.com
[21] TSC Electronics, Ltd. Technical Information [Online]. Available: http://www.tscgroup.com

Manuscript received May 12, 2005; revised September 30, 2005 (e-mail: sgoran@uns.ns.ac.yu).

Mirjana S. Damnjanović (S’02) received the B.S. and M.Sc. degrees in electrical engineering from the Faculty of Technical Sciences (FTS), University of Novi Sad, Yugoslavia, in 1994 and 2002, respectively.

In 1994, she began working in the Department of Electronics at FTS as a Research Assistant. Her research interests include modeling and optimization inductive displacement sensor, multilayer ferrite inductors, and EMI suppressors.

Goran M. Stojanović (M’04) was born on January 21, 1972. He received the B.S., M.Sc., and Ph.D. degrees in electrical engineering from the Faculty of Technical Sciences (FTS), University of Novi Sad, Yugoslavia, in 1996, 2002, and 2005, respectively.

He started his career in 1996 with FTS, Novi Sad, Yugoslavia, where he worked as a Research Assistant until 2005. He is currently an Assistant Professor teaching courses on fundamental electronics and microelectronics at the University of Novi Sad. His research interests are modeling and optimization integrated spiral inductors and transformers, modeling, and characterization of integrated passive devices and computer-aided design of integrated passive devices. He is author or coauthor of over 35 scientific papers in international journals and conferences.

Vladan D. Desnica (A’00) was born in Negotin, Serbia, Yugoslavia, on May 19, 1972. He received the B.S., M.Sc., and Ph.D. degrees in electrical engineering from the Faculty of Technical Sciences, University of Novi Sad, Yugoslavia, in 1997, 1999, and 2002, respectively.

He joined the Faculty of Technical Sciences, Novi Sad, Yugoslavia, in 2003 as an Assistant Professor. His research interests include the analysis, design, and modeling of thick-film components and symmetrical EMI/EMC filters.

Dr. Desnica is a member of IMAPS and the Yugoslav Power Electronic Society.

Ljiljana D. Živanov was born in Kragujevac, Serbia, Yugoslavia, in 1950. She received the B.S., M.Sc., and Ph.D. degrees in electrical engineering from the University of Belgrade, Belgrade, Yugoslavia, in 1974, 1980, and 1989, respectively.

She joined the Faculty of Technical Sciences, Novi Sad, Yugoslavia, in 1976 as a Teaching Assistant, and in 1990 she became an Assistant Professor. She is now a Full Professor of microelectronics at the University of Novi Sad. She has authored and coauthored over 100 papers in scientific journals and conferences in the area of modeling and simulation of electrical performance of electronic materials and devices.

Ramesh Raghavendra was born in India. He received the Ph.D. degree in material technology.

He currently is serving as a Materials Technologist, Suppression Business Unit, at Littelfuse Ireland Limited, Dundalk, Ireland. His research interests include synthesis and characterization of ceramic nano-powders for electro-ceramic applications, de-agglomeration and green body preparation methodologies for fabricating pellets from nano powders, and identification of suitable binder, solvent and disp.

Pat Bellew is a Senior Test Engineer with Littelfuse Ireland Limited, Dundalk, Ireland. He has more than 20 years of experience in the testing a characterizing of power semiconductors and metal oxide varistors. He is presently engaged mostly with multilayered varistors. He has written and presented papers on the characterization of surface mount varistors for ESD suppression.

Neil Mcloughlin was born in Ireland. He received the Ph.D. degree in electrical engineering.

He currently is serving as a Manufacturing Manager at Littelfuse Ireland Limited, Dundalk, Ireland.